ELUCIDATING PHYTOPLANKTON ASSEMBLAGE RESPONSES TO NITROGEN FORM FOLLOWING COVID-19 STAY-IN-PLACE ORDERS AT THE EAST RIVER AND LONG ISLAND SOUND CONFLUENCE

A Final Report of the Tibor T. Polgar Fellowship Program

Maximillian A. Brown

Polgar Fellow

The School of Earth and Environmental Sciences
Queens College
City University of New York
Queens, NY 11367

Project Advisor:

Dianne I. Greenfield
Environmental Sciences Initiative
Advanced Science Research Center at the Graduate Center
New York, 10031 and
The School of Earth and Environmental Sciences
Queens College
City University of New York
Queens, NY 11367

Brown, M.A., and D.I. Greenfield. 2022. Elucidating Phytoplankton Assemblage Responses to Nitrogen Form Following COVID-19 Stay-In-Place Orders at the East River and Long Island Sound Confluence. Section V:1-34 pp. *In* D.J. Yozzo, S.H. Fernald, and H. Andreyko (eds.), Final Reports of the Tibor T. Polgar Fellowship Program, 2021. Hudson River Foundation.

ABSTRACT

Nitrogen (N) form and concentration impact phytoplankton growth, harmful algal bloom formation, and hypoxia in the urbanized Long Island Sound (LIS) estuary. LIS receives N from atmospheric deposition, groundwater, remineralization, wastewater effluent, and other sources. Wastewater inputs, particularly from the East River, remain major N-contributors despite management efforts that reduced loadings; however, linkages between N form, phytoplankton species composition, and growth rates remain unclear. COVID-19 (beginning March 2020) reduced N-pollution from fossil fuel combustion and potentially changed wastewater patterns, altering coastal N-cycling. This study assessed phytoplankton responses to inorganic and organic N-forms using 2021 *in-situ* bioassays deployed at the East River/LIS border (Throgs Neck). Phytoplankton biomass as chlorophyll *a* (chl-*a*), species abundances, and growth rates were determined following 24- and 72-hour incubations. Results showed that picoplankton (<5 μm) contributed the most to overall chl-*a* in all treatments, while the diatom *Thalassiosira* spp. and cryptophytes were also abundant. N form had no significant effect on chl-*a* size fraction growth and cell concentrations, though cryptophyte growth rates were significantly greater in +urea than control treatments after 24 hours. Results suggest positive linkages between diatoms and inorganic N, supporting prior research. Analysis of publicly available data revealed significant decreases in ammonia concentrations (~5 μM, $p < .01$) during summer 2020 when compared to seasonal means. Results suggest that potential shifts in N dynamics at Throgs Neck during the COVID-19 stay-in-place period were either insufficient to measurably impact the affiliated phytoplankton

assemblages and/or the location was already over-enriched, though continuing research examines phytoplankton-N processes in other LIS regions.

TABLE OF CONTENTS

LIST OF FIGURES AND TABLES

INTRODUCTION

The urbanized Long Island Sound (LIS) is a large (average 160 km x 20 km length x width) nitrogen (N) limited estuary with an estimated 23 million people living within 80 km of the watershed (Vaudrey 2017; Vlahos et al. 2020; Long Island Sound Study 2021). LIS receives freshwater inputs from seven major rivers (the largest by volume the Connecticut River), groundwater, and tidally exchanges water with both the Atlantic Ocean (eastern boundary) and the Hudson River (western boundary) (O'Donnell et al. 2014). Approximately 9% of the total N load in LIS comes from point source sewage inputs (Vaudrey 2017), with combined freshwater inputs and atmospheric deposition delivering 20 and 3.2 x 10^6 kg N/year, respectively (Vlahos et al. 2020). The East River (considered separately as a tidal strait) delivers an estimated 3.2 x 10^6 kg N/year, of which 97% is from wastewater treatment (WWT) plants that account for 60% of the wastewater flowing out of New York City (NYC) (Vaudrey 2017).

Seasonal (summer) bottom water hypoxia recurs in the LIS, particularly in the Western Long Island Sound (WLIS) near NYC, and has been positively correlated with wind speed, N concentration, and phytoplankton biomass (chlorophyll *a*, chl-*a*) (O'Donnell et al. 2014). While hypoxic area varies with water column mixing due to physical processes, elevated N inputs also increase primary production, leading to heightened biological oxygen demand (O'Donnell et al. 2014; Whitney and Vlahos 2021). Hypoxia in LIS has been documented since the 19th century; however, the total area of hypoxic extent has decreased by ~50% since 1994 (Whitney and Vlahos 2021). This is largely due to a 58% reduction in total maximum daily loads (TMDLs) of total N (TN) associated with upgrades in four East River WWT plants, as hypoxia typically begins in

the LIS narrows before propagating eastward (Anderson and Taylor 2001; Vaudrey 2017; Vlahos et al. 2020; Whitney and Vlahos 2021). Still, the East River was recently estimated to contribute an average 11% of the entire LIS's annual N load, with a very high (±70%) degree of interannual variability from 1999-2016 (Vlahos et al. 2020). Although upgrades have reduced the N load to the full LIS, organic N from secondary treatment of East River sewage effluent may have become increasingly biologically available to micro-organisms in the WLIS following WWT upgrades (Suter et al. 2014; Yao et al. 2019; Whitney and Vlahos 2021). High levels of suspended inorganic matter and low chl-*a* levels suggest that the East River is light limited and may supply N to the WLIS where water clarity does not limit phytoplankton growth (Li et al. 2018).

Coastal enrichment of N can stimulate increases in phytoplankton cell abundances and biomass in estuaries, sometimes contributing to the proliferation of harmful algal blooms (HABs) (Anderson et al. 2008; Hattenrath-Lehmann et al. 2015, 2017; Griffith et al. 2019). Distinct chemical forms and concentrations of N differentially influence phytoplankton growth and community structure (Cira et al. 2016; Reed et al. 2016). The LIS provides a local system to study the sensitivity of phytoplankton assemblages to N form and concentration along a gradient of increasing urbanization. Since 2002, the relative proportions of major phytoplankton taxa in LIS have been routinely analyzed using high performance liquid chromatography (HPLC) photopigment analysis (Suter et al. 2014). During this period (2002-2014), it is believed that phytoplankton assemblages in the WLIS have responded to decreases in WWT loadings and shifts in the concentrations of available N-form, particularly as dissolved inorganic nitrogen (DIN) became relatively less available than dissolved organic N (DON) (Suter et al. 2014).

The decrease in DIN availability in the WLIS over the past two decades is relevant because diatoms rapidly assimilate oxidized forms of DIN (Olofsson et al. 2019) and constitutively express nitrate (NO_3^-) transporters even in the presence of alternate N sources (Song and Ward 2007). Since the 1950s, WLIS and East River phytoplankton assemblages have been primarily (>70% in the East River) composed of diatoms (Li et al. 2018), with seasonal WLIS blooms dominated by *Skeletonema costatum* (documented now as a cryptic species, Lopez et al. 2014) and *Thalassiosira* spp. (O'Shea and Brosnan 2000). By comparison, reduced DIN as ammonia (NH_3) has been shown to inhibit diatom growth in some estuarine systems (Glibert et al. 2014). In the WLIS, blooms of the toxic dinoflagellate *Dinophysis acuminata* have been linked to high ammonium (NH_4^+) levels (Hattenrath-Lehmann et al. 2015).

Elevated concentrations of dissolved organic N (DON) have been associated with dinoflagellate blooms (Heil et al. 2007). Through osmotrophy, dinoflagellates can flexibly uptake a wide range of organic molecules from their surrounding environments (Glibert and Legrand 2006). Bioassay results have shown N-additions, especially organic N, result in elevated phytoplankton biomass in tidal creek estuaries near urban areas when compared to less developed locations (Reed et al. 2016). In the 21st Century there have been new summer abundance peaks for several dinoflagellates in LIS, such as *Prorocentrum triestinum*, *P. micans*, and *P. minimum* (Lopez et al. 2014), with blooms of the latter reported in response to anthropogenic sources of DON in several marine environments (Glibert and Legrand 2006). Over the past decade, blooms of the icthyotoxic *Margalefidinium polykrikoides* and the saxitoxin-producing genus *Alexandrium* have been documented in the LIS region (Hattenrath-Lehmann et al. 2017;

Griffith et al. 2019). Blooms of *M. polykrikoides* have been associated with high organic N concentrations in the eastern LIS (Gobler et al. 2012), and a bloom of *A. catenella* was associated with WWT effluent from a Northport discharge site in 2008 (Hattenrath et al. 2010); however, *A. catenella* has also shown preferential growth response to ammonia in culture, highlighting the importance of localized growth conditions in nutrient linkages (Armstrong et al. 2018).

These examples suggest that relatively higher concentrations of DON have contributed to a decrease in the relative proportion of diatoms in the total LIS phytoplankton assemblage (Suter et al. 2014). It has also been hypothesized that smaller cells (picoplankton/cyanobacteria) may more readily take up lower concentrations of DIN (NO_3^- and NH_4^+) and should have therefore increased in abundances (Suter et al. 2014). While changes in localized phytoplankton assemblages can be attributed to shifts in available LIS N forms, there appears to have been no clear trend in total chl-*a* concentration when considering the LIS as whole since TMDLs were implemented (Whitney and Vlahos 2021). Furthermore, much of the WLIS remains hypoxic mid-July through August (with a large degree of inter-annual variability), and the relationship between both N form and concentration on oxygen concentration remains poorly understood in this system (Whitney and Vlahos 2021). Understanding how different N-forms impact WLIS phytoplankton populations and stimulate bloom events could help clarify the mechanism(s) by which reductions in N load have impacted seasonal hypoxia.

A New York State disaster emergency was in place from March 7, 2020, to June 24, 2021 with stay-in-place orders in response to the COVID-19 pandemic. Atmospheric NO_x concentrations in the New York City (NYC) metropolitan area in March 2020 were

24% percent lower relative to the 2015-2019 mean (Connerton et al. 2020). The pandemic may also have affected patterns in nutrient-rich wastewater inputs, as the number of employees working from home within the United States during 2020 was estimated to increase from 8.2% to 35.2% (February – May 2020) (Bick et al. 2020). Combined, these probable shifts in overall N inputs provide a unique opportunity to test the hypothesis that major changes in human activity can impact coastal nutrient forms and levels, and thus phytoplankton assemblages. This information may further elucidate mechanisms linking coastal N enrichment with algal bloom dynamics.

To test this hypothesis, this study attempts to achieve the following goals and objectives:

Goal and Objectives

Goal: Assess phytoplankton assemblage dynamics at the East River/LIS border following COVID-19 stay-in-place orders as they relate to fluctuations in N form and concentration.

Objective 1: Quantify phytoplankton assemblage responses to N-form via an *in-situ* bioassay.

Objective 2: Document phytoplankton species composition at the East River/LIS border during summer 2021.

METHODS

Study Area and Historical Characteristics

From July 2021 to September 2021, bioassay incubations and interim sampling took place at the SUNY Maritime Pier on Throgs Neck and at the nearby Soundview Pier, respectively (Figure 1). These sites were each selected to capture water entering the LIS from the Hudson River Estuary, as Throgs Neck demarcates the boundary between the WLIS and East River. Historical data from the New York City Department of Environmental Protection (NYC DEP) station E8 were used to assess seasonal ranges in concentration for N forms in the study area (NYC DEP 2021). Specifically, mean nitrite (NO_2) + nitrate (NO_3^-) (henceforth N+N) and ammonium (NH_4^+) values (2010-2019 as pre-COVID and 2020 as COVID concentrations) were downloaded. (https://data.cityofnewyork.us/Environment/Harbor-Water-Quality/5uug-f49n).

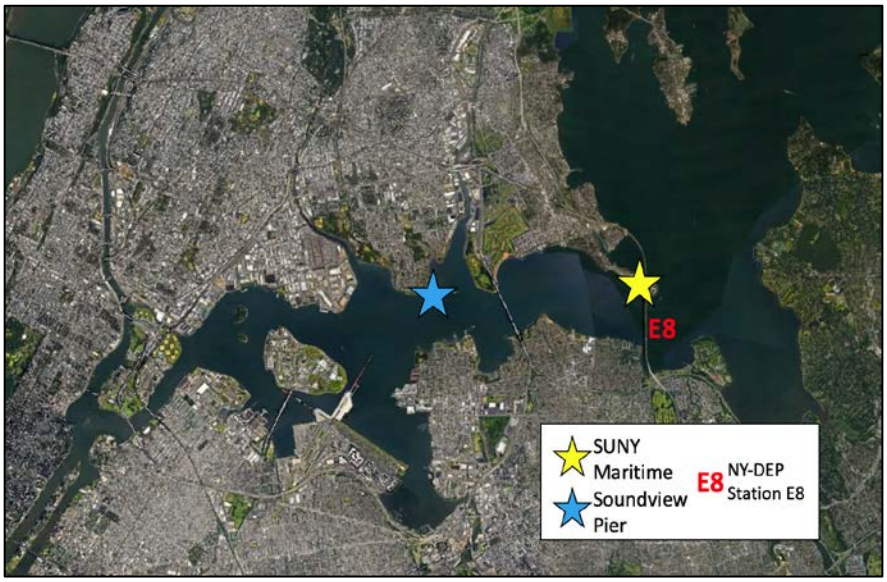

Figure 1: Study Area at the East River/LIS border. Field sampling occurred at SUNY Maritime on Throgs Neck and Soundview Pier. The Throgs Neck nutrient addition bioassay was deployed at SUNY Maritime.

In Situ Bioassays

To address Objective 1, a nutrient addition bioassay was conducted to elucidate how different N forms impact phytoplankton biomass and species composition at the westernmost part of the LIS. Experiments were conducted *in situ* (native light and temperature conditions) from a floating dock at SUNY Maritime from September 7th to September 10, 2021 (Figure 1). N was added (+20 µM per atom of N) as either ammonium, nitrate, or urea, to represent reduced, oxidized, and organic N, respectively. These concentrations placed nitrate and ammonia concentrations above the summer historical ranges (calculated from seasonal means using 2010-2019 NYC DEP publicly available data; Figure 2). Phosphorus (P) was then added as orthophosphate at 'Redfield' stoichiometric ratios (16:1 N:P per atom) to avoid P co-limitation (Redfield 1958; Reed et al. 2015, 2016; Sitta et al. 2018). There were six treatments total with three replicates per treatment: ammonium and phosphate (AP), nitrate and phosphate (NP), urea and phosphate (UP), all-nutrients and phosphate (ALL), phosphate only (P), and a control with no additions (CTRL).

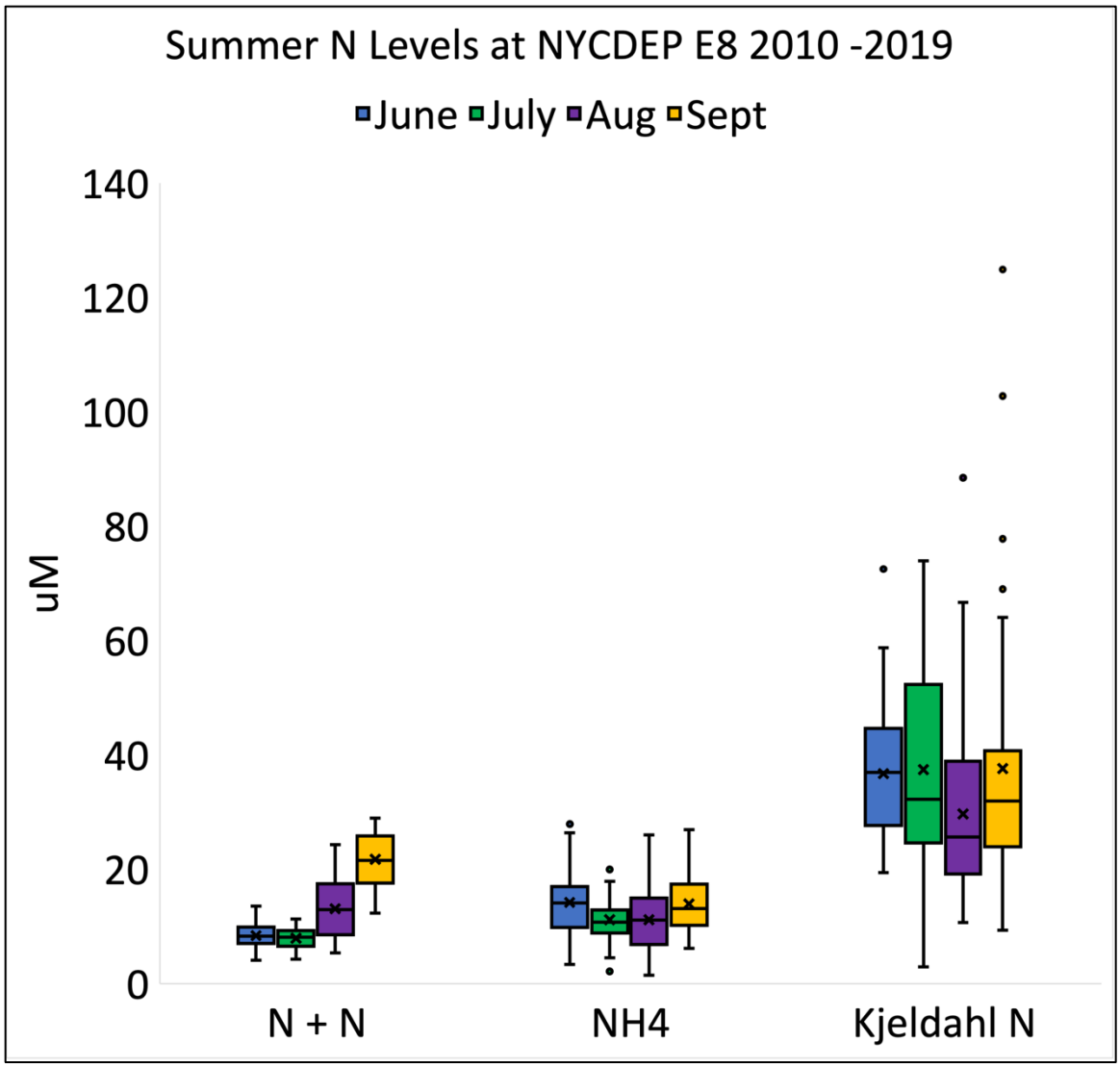

Figure 2: **Ranges in summer N form and concentration at Throgs Neck NYC DEP station E8. Data are shown from 2010-2019 to capture the decade prior to COVID-19. N+N = (NO_2 + NO_3^-). Kjeldahl N is the sum of organic N and N in both NH_3 and NH_4^+. Data source: NYC DEP 2021.**

Bioassay deployment and surface water collections at SUNY Maritime on Throgs Neck occurred two hours before low tide (approximately 16:10 on September 7, 2021). At the start of each experiment (t0), whole water was collected from 0.5 m depth, and dispensed into previously acid-washed (10% HCl for > 4 hours and rinsed three times with RO water) 2L polycarbonate bottles that were rinsed with surface water onsite. Nutrients were then added to 2L bottles according to the above-described treatments to

achieve a final concentration increase of +20 µM per atom of N. Bottles were secured to the dock in a large mesh bag to block 60-70% surface irradiance and avoid photoquenching of phytoplankton cells (Reed et al. 2015, 2016; Sitta et al. 2018), then incubated *in situ* at the water's surface for 72 hours. This incubation time frame effectively assessed community composition changes without a risk of nutrient depletion (Siegel et al. 2011). At t(0), 1L surface water samples were also collected (*n*=3), and then each treatment was sub-sampled at t(24) (post-24 hours, to capture short-term N uptake) and t(72) (final, to capture assemblage shifts). All samples were analyzed for nutrients (total dissolved N + P (TDN and TDP), NO_2^- + NO_3^-, NH_4^+, and SiO_4^{4-}), chl-*a* (at total, <20 µm, and <5 µm size fractions) and phytoplankton (species identifications and counts). Nutrients, phytoplankton, and chl-*a* were analyzed as described below. Physical water quality (temperature - T, pH, dissolved oxygen - DO, salinity - S, and turbidity) was recorded from surface water at t(0) and t(72) point using a YSI handheld data sonde, a handheld pH meter, and a Secchi disk.

Field sampling

To address Objective 2 and provide ecological context for Objective 1, additional water samples were collected on July 12 from SUNY Maritime, and on August 4 and 17 from Soundview. For all collections, samples (0.3-0.5 m depth) were obtained with acid washed (10% HCl for > 4 hours and rinsed three times with RO water) 1L opaque Nalgene bottles (*n*=3), kept cool and in the dark, and then transported to the laboratory for phytoplankton cell counts.

Analytical methods

Nutrient Analysis

Each replicate was filtered (0.7 μm glass fiber filters (GF/Fs)) into acid washed (10% HCl for > 4 hours and rinsed three times with DI water) 20 mL glass scintillation vials for analysis of TDN, TDP, NH_4^+, $NO_2 + NO_3^-$, and PO_4^{3-}. Dissolved SiO_4^{4-} was similarly processed, but filtrate was stored in plastic scintillation vials. Unfiltered water samples were collected in glass scintillation vials for analysis of total N and P (TN and TP). All nutrient samples were then frozen (-20 °C) before analysis with a Lachat +8500 autoanalyzer (Zimmerman and Keefe 1991; Grasshoff et al. 1999; Hales et al. 2004). DON and dissolved organic P (DOP) were calculated by subtracting the combined dissolved inorganic N and P pools from TDN and TDP, respectively.

Phytoplankton Counts

Aliquots (20 mL) for each replicate were fixed to a 1% dilution with Lugol's iodine solution into 20 mL glass amber vials and refrigerated until analysis. All replicate samples were subsequently evaluated via microscopy for species composition and abundances to the lowest taxonomic level possible. Cells were enumerated with a Sedgewick rafter chamber (nano- and microplankton) until ≥300 cells per species or the entire chamber was counted, whichever occurred first, on an Olympus CKX53 inverted light microscope.

Growth Rates

Instantaneous growth rates per species were calculated from the following formula for phytoplankton counts where *X* is the concentration of cells at timepoint *t* (Reed et al. 2016):

$$\frac{lnX_{t2} - lnX_{t1}}{\Delta t}$$

Pigment Analysis

For all replicates, chl-*a* concentration was quantified as a proxy for phytoplankton biomass by condensing 40 mL aliquots of water samples on to GF/Fs according to total, <20 μm, and <5 μm size fractions via filteration through Nitex nylon mesh screens to determine relative contributions of micro, nano, and pico-phytoplankton to overall biomass (Greenfield et al. 2005; Lonsdale et al. 2006). All pigment samples were stored at -20°C until analysis following standard procedures (Welschmeyer 1994). .

Statistical Analysis

All data were tested for normality (Shapiro-Wilk) prior to analyses. R Studio (v1.4.1106) was used for statistics. A significance level of $\alpha = 0.05$ was used for all analyses unless otherwise noted.

Historical N-values at NY-DEP station E8

Mean N+N and ammonium (NH_4^+) values (2010-2019, pre COVID-19) were compared to summer (June through September) 2020 N concentrations (during COVID-19) using two sample T-tests.

In-Situ Bioassays

Phytoplankton species abundances and chl-*a* concentrations were compared between each experimental treatment and the control at 72 hours using a one-way ANOVA. Differences in growth rates between both t(72) and t(24) as well as t(24) and t(0) were compared using a one-way ANOVA containing each replicate. Differences among groups for chl-*a* levels at three size fractions (<5 μm, 5-20 μm, >20 μm, as well as total (all size fractions combined)) were compared using both one-way ANOVAs and paired T-tests for all replicates with respect to the control.

RESULTS

Pre- and post-COVID-19 N form and concentration at NY-DEP Station E8

Values of N+N during June 2020 indicated a weakly significant (two sample T-test, at $\alpha = 0.1$; p=.086) decrease from historical values at Throgs Neck (Table 1). During 2020, values for NH_4^+ were significantly less than mean historical values for June (paired T-test, 10.10 μM versus 14.23 μM, p=.024), and during September this reduction was highly significant (two sample T-test, 7.45 μM versus 13.99 μM, $p = 2.87e^{-05}$).

Bioassay biomass and phytoplankton community changes

At t0, water quality was recorded as temperature (24°C), salinity (24.15 PSU), DO (5.03 mg/L), pH (8.16), and moderately turbid (Secchi depth of 1.5 m) (Table 2). Mean (n=3) chl-*a* was 0.98 μg/L in the >20 μm size fraction, 0.85 μg/L in the 5-20 μm size fraction, 2.58 μg/L in the <5 μm size fraction with a total biomass of 4.41 ± .17 μg/L (error terms represent standard error henceforth). *Thalassiosira* spp. (110 ± 8 cells/mL)

and *Skeletonema* spp. (43 ± 13 cells/mL) were the most abundant diatoms (Table 3). Few dinoflagellates were observed, though cryptophytes (251 ± 9 cells/mL) were abundant.

Table 1: Comparison of 2020 (COVID-19) concentrations of N+N (NO_2 + NO_3^-) and NH_4^+ with historical values. Significant differences are denoted as weak (asterisk; $p < 0.1$), strong (bold; $p < 0.05$), and highly significant (bold, underline; $p < 0.01$).

Month/Nutrient	Mean Pre-Covid (µM, 2010-2019)	2020 Mean (µM)	T-test Used	*p*-value
N+N June	8.43 (*n*=43)	4.75 (*n*=2)	Welch's Two Sample	.086*
N+N July	7.96 (*n*=37)	6.35 (*n*=1)	Two Sample	.382
N+N August	13.13 (*n*=43)	11.42 (*n*=3)	Welch's Two Sample	.321
N+N September	21.76 (*n*=43)	22.86 (*n*=3)	Welch's Two Sample	.774
NH_4^+ June	14.23 (*n*=43)	10.10 (*n*=2)	Welch's Two Sample	**.024**
NH_4^+ July	11.19 (*n*=37)	8.14 (*n*=1)	Two Sample	.456
NH_4^+ August	11.20 (*n*=43)	13.30 (*n*=3)	Welch's Two Sample	.719
NH_4^+ September	13.99 (*n*=43)	7.45 (*n*=3)	Welch's Two Sample	**$\underline{2.87e^{-05}}$**

Table 2: Water quality parameters recorded at t(0) and t(72) of bioassay deployment at SUNY Maritime, Throgs Neck. pH was not recorded on 9/10/21. T=Temperature, S= Salinity, PSU= Practical Salinity Unit, DO= Dissolved Oxygen.

Date (2021)	Depth (m)	T (°C)	S (PSU)	DO (mg/L)	pH	Secchi depth (m)
9/7	0.3-0.5	24.0	24.15	5.03	8.16	1.5
9/10	0.3-0.5	23.3	24.58	4.78	-	1.5

Table 3: Mean (*n*=3, except for 8/17 Soundview which was *n*=2) ± standard error (SE) of abundant microphytoplankton observed during summer 2021.

	SUNY Maritime	Soundview	Soundview	SUNY Maritime
Species/Taxa	**7/12 mean ± SE (cells/ml)**	**8/4 mean ± SE (cells/ml)**	**8/17 mean ± SE (cells/ml)**	**9/7 mean ± SE (cells/ml)**
Diatoms				
Skeletonema spp.	283.1 ± 21.2	286.8 ± 26.9	68.2 ± 5.6	42.8 ± 12.5
Thalassiosira spp.	1,742.7 ± 387.2	119.8 ±12.1	81.8 ± 9.1	110.4 ± 8.0
Guinardia sp.	92.6 ± 9.4	87.9 ± 4.6	24.7 ± 1.5	5.1 ± 2.3
Leptocylindrus sp.	12.1 ± 3.8	477.2 ± 60.6	22.7 ± 9.6	7.7 ± 3.9
Navicula spp.	20.9 ± 2.2	4.7 ± 1.7	31.8 ± 0.5	9.1 ± 0.6
Lithodesmium sp.	0.00	0.00	0.00	24.6 ± 3.3
Dinoflagellates				
Heterocapsa sp.	14.5 ± 4.9	2.0 ± 1.5	15.7 ± 3.5	0.3 ± 0.3
Scrippsiella sp.	6.4 ± 1.8	1.7 ± 0.3	4.6 ± 1.5	0.7 ± 0.3
Prorocentrum minimum	26.6 ± 8.0	0.0 ± 0.3	2.0 ± 0.0	1.0 ± 0.6
Prorocentrum micans	13.5 ± 3.2	1.0 ± 0.6	5.1 ± 1.0	3.7 ± 0.7
Other				
Cryptophytes	2.0 ± 0.6	10.8 ± 5.3	174.7 ± 50.5	251.1 ± 9.5
Euglenophytes	6.1 ± 2.1	75.1 ± 4.4	5.0 ± 0.0	2.4 ± 1.2

At t(72), picoplankton were the greatest contribution to total phytoplankton biomass in the control treatment, as chl-*a* concentrations averaged 2.51 µg/L in the >20 µm size fraction, 1.40 µg/L in the 5-20 µm size fraction, and 6.07 µg/L in the <5 µm size fraction with a total biomass of 9.98 ± 3.04 µg/L (Figure 3). There were no significant differences in chl-*a* values for each size fraction between each nutrient addition (one way-ANOVA; $p > 0.05$). Paired T-tests between each nutrient treatment and the control indicated significant decreases in biomass at the <5 µm size fraction for the UP (mean chl-*a*: 3.8 µg/L, p=.02) and ALL treatments (mean chl-*a*: 4.2 µg/L, p=.05) (Table 4). Mean growth rates for all chl-*a* size fractions and totals were not significantly different across all time points (one way-ANOVA; data not shown).

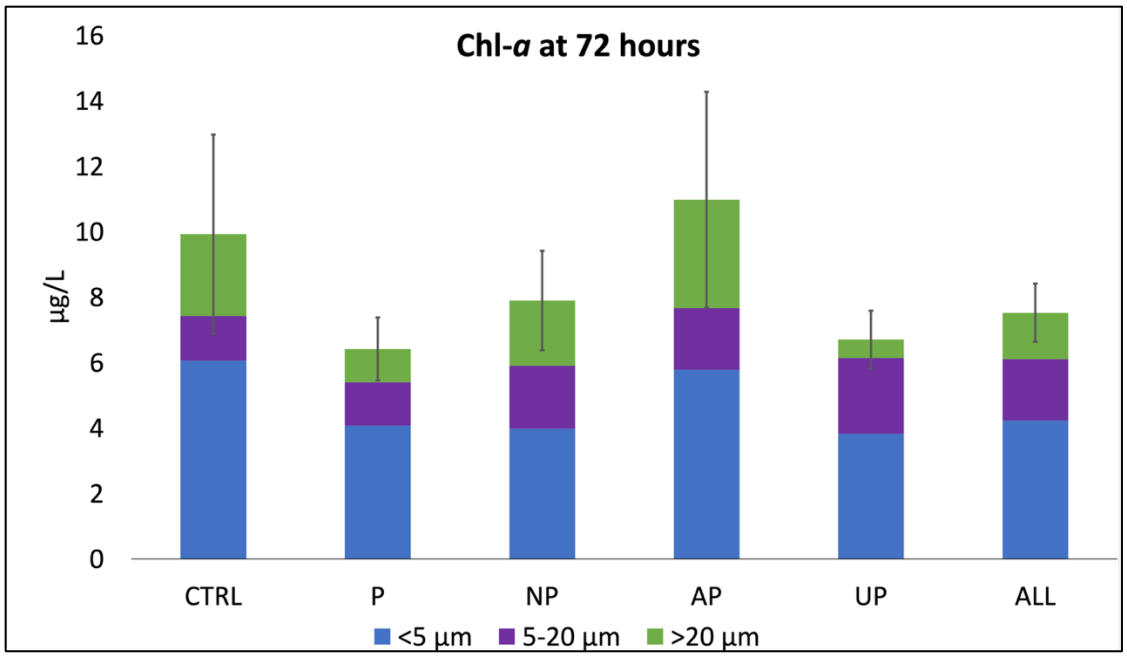

Figure 3: **Final t(72) chl-*a* concentrations by size fraction across treatments from Throgs Neck bioassay. Error bars represent one standard error above and below the mean for chl-*a* totals.**

Table 4: **Results of paired T-tests (*p*-values) with respect to control for final t(72) chl-*a* concentrations at each size fraction from the Throgs Neck bioassay. Significant differences are denoted as bold; $p < 0.05$.**

	Treatment				
Size Fraction	P	NP	AP	UP	ALL
<5 µm	.17	.42	.68	**.02**	**.05**
5-20 µm	.98	.73	.76	.53	.73
>20 µm	.46	.79	.79	.36	.58
Total	.37	.60	.83	.40	.52

At t(72), *Thalassiosira* spp. (558 ± 143 cells/mL), *Skeletonema* spp. (291 ± 141 cells/mL), and *Lithodesmium* sp. (242 ± 13 cells/mL), were the most abundant diatoms in the control (Table 5, Figure 4). In addition, *Heterocapsa* sp. (3 ± 3 cells/mL), *P. triestinum* (3 ± 2 cells/mL), and *Gymnodinium* sp. (2 ± 2 cells/mL) were the most

abundant dinoflagellates in the control, and cryptophytes were observed at mean concentrations of 26 ± 11 cells/mL. One-way ANOVAs indicated no significant differences between mean cell concentrations of each treatment for each observed species and taxonomic grouping at t(72) apart from *P. minimum* (p=.05), and post-hoc analyses (Tukey) indicated no significant differences between each treatment and the control for this species.

Instantaneous growth rates between t(24) and t(0) counts of each observed species and taxonomic grouping indicated several significant differences across treatments (Table 5). *Heterocapsa* sp. growth rates across treatments had significant differences (one-way ANOVA, p<.01). Post-hoc analysis (Tukey) indicated highly significant (p<.01) increases between both the UP and P treatments compared to the control, and paired T-tests indicated significant increases between the NP (p=.03), UP (p<.01) and P (p<.01) treatments compared to the control. *Gymnodinium* sp. growth rates across treatments had significant differences (one-way ANOVA, p=.01). Post-hoc analysis (Tukey) indicated a significant decrease between the ALL treatment (p=.04) when compared to the control, and paired T-tests corroborated this (p<.01). Unidentified dinoflagellate (not assigned species or taxa due to damage or obfuscation) growth rates across treatments were significantly different (one-way ANOVA, p<.01). Post-hoc analysis (Tukey) indicated no significant differences between nutrient additions when compared to the control. Cryptophyte growth rates across treatments had significant differences (one-way ANOVA, p<.01). Post-hoc analysis (Tukey) indicated significant increases in the UP treatment when compared to the control (p=.02) and significant decreases in the ALL

treatment when compared to the control (p=.03), with paired T-tests corroborating these values (p=.04 and p=.03, respectively).

Growth rates between t(24) and t(72) for each observed species and taxonomic grouping only contained significant differences in the mean growth rates of cryptophytes (one-way ANOVA, p=.03, Table 5). Post-hoc analysis (Tukey) indicated no significant differences between nutrient additions when compared to the control.

Table 5: Mean (*n*=3 per treatment ± SE) final cell concentrations and growth rates (t(0) to t(24) and t(24) to t(72)) for the most abundant species/taxonomic groupings in each Throgs Neck bioassay treatment. Significant differences are denoted as strong (bold; $p < 0.05$), and highly significant (bold, underline; $p < 0.01$). CTRL= control, P= Phosphate, NP= Nitrate and Phosphate, AP= Ammonium and Phosphate, UP=Urea and Phosphate, ALL= ALL nutrient additions.

Species/Taxa	Treatment	t(72) mean ± SE (cells/mL)	ANOVA p-value	Growth Rate t(0) to t(24) ± SE	ANOVA p-value	Growth Rate t(24) to t(72) ± SE	ANOVA p-value
Diatoms							
Skeletonema spp.	CTRL	291.5 ± 140.6	0.58	0.046 ± 0.004	0.81	0.011 ± 0.011	0.19
	P	97.2 ± 29.0		0.046 ± 0.007		-0.008 ± 0.005	
	NP	309.5 ± 68.3		0.043 ± 0.004		0.020 ± 0.008	
	AP	408.5 ± 193.9		0.040 ± 0.005		0.021 ± 0.010	
	UP	166.8 ± 70.8		0.049 ± 0.002		0.000 ± 0.009	
	ALL	279.4 ± 137.4		0.039 ± 0.009		0.015 ± 0.006	
Cylindrotheca spp.	CTRL	40.2 ± 10.1	0.58	0.083 ± 0.005	0.31	0.004 ± 0.007	0.90
	P	29.5 ± 8.4		0.096 ± 0.002		-0.010 ± 0.006	
	NP	36.2 ± 22.1		0.076 ± 0.012		0.004 ± 0.006	
	AP	65.0 ± 24.6		0.093 ± 0.007		0.005 ± 0.015	
	UP	40.2 ± 12.9		0.105 ± 0.007		-0.009 ± 0.011	
	ALL	26.8 ± 13.2		0.077 ± 0.018		-0.007 ± 0.020	
Navicula spp.	CTRL	57.6 ± 9.9	0.98	0.030 ± 0.007	0.58	0.023 ± 0.007	0.34
	P	41.5 ± 4.7		0.038 ± 0.003		0.013 ± 0.004	
	NP	48.2 ± 4.0		0.037 ± 0.005		0.017 ± 0.003	
	AP	44.2 ± 16.9		0.029 ± 0.001		0.015 ± 0.009	
	UP	48.9 ± 15.1		0.033 ± 0.005		0.016 ± 0.010	
	ALL	21.1 ± 1.0		0.041 ± 0.007		-0.005 ± 0.004	
Thalassiosira spp.	CTRL	557.8 ± 143.3	0.35	0.052 ± 0.001	0.28	0.006 ± 0.006	0.21
	P	492.5 ± 81.3		0.055 ± 0.004		0.003 ± 0.002	
	NP	857.7 ± 93.4		0.050 ± 0.002		0.019 ± 0.002	
	AP	994.3 ± 299.7		0.052 ± 0.001		0.017 ± 0.008	
	UP	596.3 ± 123.7		0.057 ± 0.004		0.006 ± 0.006	
	ALL	812.0 ± 171.4		0.044 ± 0.006		0.019 ± 0.005	
Chaetoceros spp.	CTRL	16.1 ± 6.1	0.63	0.000	-	0.001 ± 0.002	0.52
	P	4.0 ± 4.0		0.000		0.005 ± 0.005	
	NP	0.0		0.000		0.000	
	AP	12.1 ± 12.1		0.000		0.008 ± 0.008	
	UP	9.4 ± 5.2		0.000		0.000	
	ALL	4.0 ± 4.0		0.000		-0.004 ±0.004	
Leptocylindrus sp.	CTRL	32.8 ± 9.5	0.59	0.042 ± 0.005	0.36	0.007 ± 0.010	0.33
	P	6.7 ± 4.8		0.059 ± 0.002		-0.020 ± 0.013	
	NP	12.1 ± 6.0		0.055 ± 0.013		-0.020 ± 0.022	
	AP	24.1 ± 12.9		0.054 ± 0.013		0.000 ± 0.002	
	UP	14.7 ± 7.7		0.057 ± 0.009		-0.003 ± 0.002	
	ALL	21.4 ± 15.8		0.032 ± 0.009		0.003 ± 0.007	
Guinardia sp.	CTRL	30.2 ± 14.1	0.42	0.075 ± 0.009	0.14	-0.010 ± 0.020	0.29
	P	27.5 ± 17.2		0.077 ± 0.010		-0.018 ± 0.017	
	NP	57.3 ± 9.0		0.085 ± 0.002		0.007 ± 0.003	
	AP	60.3 ± 19.8		0.069 ± 0.011		0.014 ± 0.007	
	UP	34.2 ± 12.3		0.088 ± 0.003		-0.008 ± 0.010	
	ALL	61.6 ± 14.6		0.056 ± 0.009		0.023 ± 0.009	
Paralia sp.	CTRL	25.5 ± 6.0	0.32	0.000	0.65	0.000	0.79
	P	10.1 ± 3.1		-0.018 ± 0.005		0.013 ± 0.007	
	NP	2.0 ± 2.0		-0.003 ± 0.004		-0.004 ± 0.004	
	AP	22.8 ± 20.8		-0.010 ± 0.017		0.009 ± 0.013	
	UP	40.2 ± 12.8		-0.001 ± 0.001		0.015 ± 0.015	
	ALL	13.4 ± 3.5		-0.013 ± 0.013		0.010 ± 0.010	
Lithodesmium sp.	CTRL	242.2 ± 13.1	0.82	0.054 ± 0.003	0.16	0.019 ± 0.003	0.75
	P	198.3 ± 9.5		0.062 ± 0.002		0.013 ± 0.001	

	NP	297.5 ± 88.4		0.057 ± 0.008		0.019 ± 0.008	
	AP	302.2 ± 132.9		0.048 ± 0.006		0.022 ± 0.010	
	UP	223.1 ± 29.6		0.050 ± 0.003		0.021 ± 0.002	
	ALL	214.4 ± 67.7		0.040 ± 0.007		0.023 ± 0.006	
Dinoflagellates							
Heterocapsa sp.	CTRL	2.7 ± 2.7	0.68	0.031 ± 0.015	**<.01**	0.000	0.15
	P	1.3 ± 0.7		0.150 ± 0.008		-0.027 ± 0.014	
	NP	3.0 ± 1.0		0.093 ± 0.011		-0.002 ± 0.017	
	AP	0.7 ± 0.7		0.061 ± 0.031		-0.003± 0.003	
	UP	0.0		0.151 ± 0.009		0.000	
	ALL	1.3 ± 1.3		0.000		0.000	
Scrippsiella sp.	CTRL	0.0	0.51	0.000	0.24	0.000	-
	P	0.0		0.036 ± 0.019		0.000	
	NP	0.0		0.000		0.000	
	AP	0.0		0.027 ± 0.019		0.000	
	UP	0.0		0.027 ± 0.019		0.000	
	ALL	0.7 ± 0.7		0.000		0.000	
Gymnodinium sp.	CTRL	2.0 ± 2.0	0.82	-0.003 ± 0.001	**0.01**	0.005 ± 0.005	0.16
	P	2.0 ± 2.0		0.000		0.000	
	NP	0.0		-0.017 ± 0.017		0.000	
	AP	1.3 ± 1.3		0.000		0.000	
	UP	0.0		-0.033 ± 0.017		0.000	
	ALL	2.0 ± 1.2		-0.050 ± 0.000		0.014 ± 0.008	
Prorocentrum minimum	CTRL	0.7 ± 0.7	**0.05**	0.010 ± 0.010	0.47	0.000	0.40
	P	0.0		0.035 ± 0.018		0.000	
	NP	3.0 ± 1.0		0.010 ± 0.010		0.014 ± 0.014	
	AP	0.7 ± 0.7		0.010 ± 0.010		0.000	
	UP	1.3 ± 0.7		0.015 ± 0.015		0.002 ± 0.007	
	ALL	0.0		0.000		0.000	
Prorocentrum triestinum	CTRL	2.7 ± 1.8	0.67	0.141 ± 0.014	0.60	-0.012 ± 0.006	0.11
	P	4.7 ± 1.3		0.160 ± 0.003		-0.028 ± 0.007	
	NP	4.0 ± 2.0		0.148 ± 0.008		-0.023 ± 0.017	
	AP	2.0 ± 2.0		0.150 ± 0.003		-0.006 ± 0.006	
	UP	2.7 ± 0.7		0.140 ± 0.010		-0.028 ± 0.004	
	ALL	1.3 ± 1.3		0.146 ± 0.007		-0.005 ± 0.005	
Unidentified Dinoflagellates	CTRL	16.1 ± 4.0	0.22	-0.066 ± 0.016	**<.01**	0.009 ± 0.007	0.20
	P	5.4 ± 2.9		-0.031 ± 0.007		-0.014± 0.009	
	NP	7.0 ± 3.0		-0.043 ± 0.003		-0.021 ± 0.007	
	AP	8.7 ± 3.5		-0.065 ± 0.005		-0.009 ± 0.015	
	UP	12.7 ± 1.8		-0.034 ± 0.012		-0.011 ± 0.007	
	ALL	8.7 ± 2.4		-0.116 ± 0.023		0.021 ± 0.016	
Other							
Euglenophytes	CTRL	6.0 ± 1.2	0.54	0.091 ± 0.010	0.34	-0.027 ± 0.008	0.22
	P	5.4 ± 2.9		0.087 ± 0.001		-0.013 ± 0.007	
	NP	0.0		0.083 ± 0.007		0.000	
	AP	4.0 ± 4.0		0.081 ± 0.007		-0.004 ± 0.004	
	UP	8.7 ± 3.5		0.096 ± 0.002		-0.027 ± 0.013	
	ALL	4.7 ± 1.8		0.077 ± 0.006		-0.027 ± 0.011	
Cryptophytes	CTRL	26.1 ± 10.6	0.26	-0.001 ± 0.006	**<.01**	-0.051 ± 0.012	**0.03**
	P	6.0 ± 4.0		0.016 ± 0.002		-0.095 ± 0.012	
	NP	18.1 ± 14.1		0.005 ± 0.005		-0.068 ± 0.018	
	AP	45.6 ± 22.1		0.004 ± 0.005		-0.045 ± 0.014	
	UP	10.1 ± 4.0		0.025 ± 0.006		-0.082 ± 0.010	
	ALL	22.8 ± 3.5		-0.026 ± 0.004		-0.037 ± 0.005	

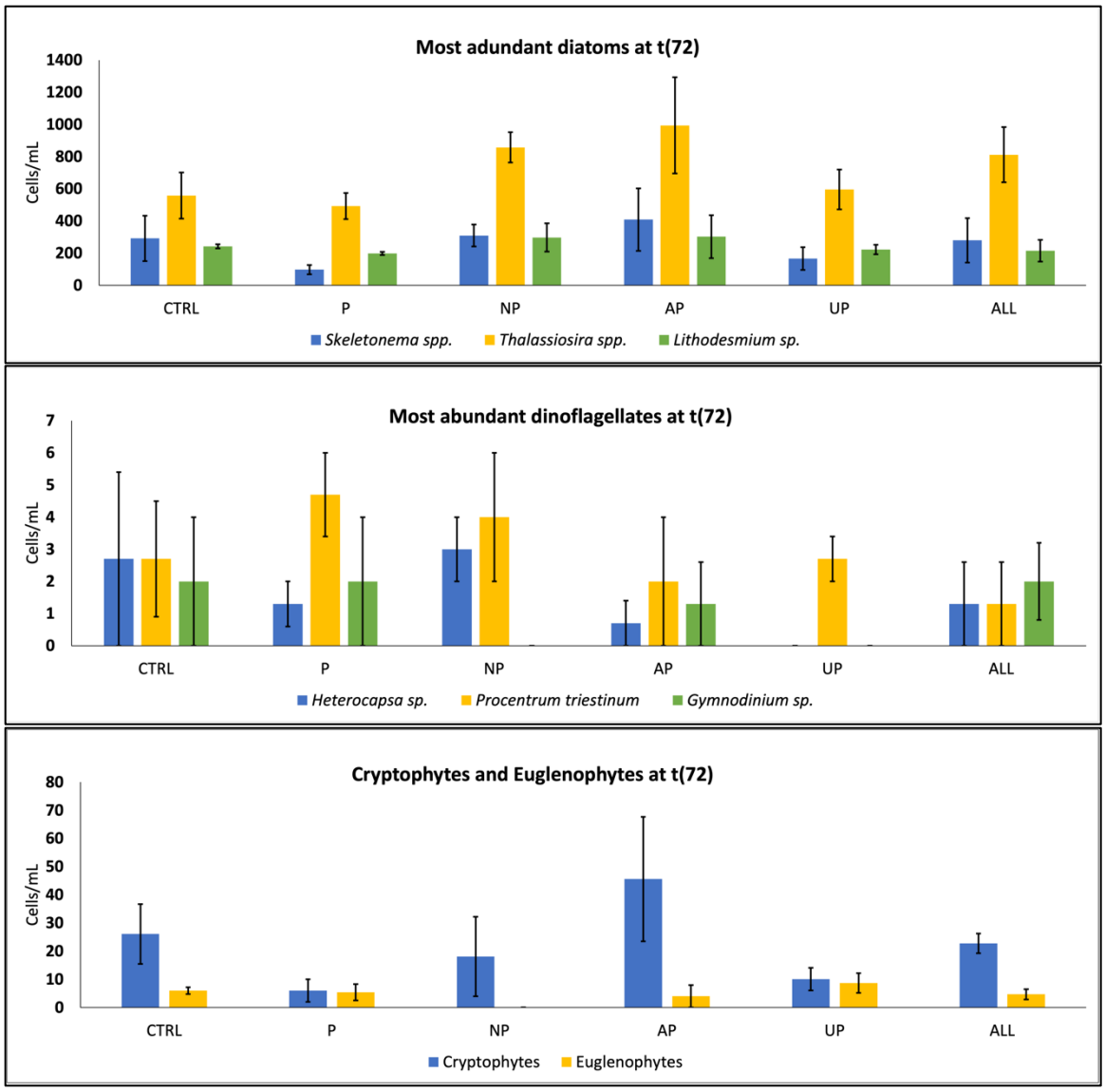

Figure 4: **Most abundant phytoplankton mean counts for diatoms, dinoflagellates, and other (euglenophytes, cryptophytes) at t(72) across all treatments in the Throgs Neck bioassay. Error bars represent one standard error above and below the mean. CTRL= control, P= Phosphate, NP= Nitrate and Phosphate, AP= Ammonium and Phosphate, UP=Urea and Phosphate, ALL= ALL nutrient additions. Note different scales in y-axes.**

Phytoplankton community at the East River/LIS border

On July 12 at SUNY Maritime, *Thalassiosira* spp. (1,743 ± 387 cells/mL), *Skeletonema* spp. (283 ± 21 cells/mL), and *Guinardia* sp. (93 ± 9 cells/mL) were the most abundant diatoms (Table 3). *Prorocentrum minimum* (27 ± 8 cells/mL), *P. micans* (13 ± 3 cells/mL), and *Heterocapsa* sp. (14 ± 5 cells/mL) were the most abundant dinoflagellates**.**

At Soundview on August 4, *Leptocylindrus* sp. (477 ± 61 cells/mL), *Skeletonema* spp. (287 ± 27 cells/mL), and *Thalassiosira* spp. (120 ± 12 cells/mL) were the most abundant diatoms. Dinoflagellates were not present in abundance, and euglenophytes were observed at concentrations of 75 ± 4 cells/mL (Table 3). On August 17, *Thalassiosira* spp. (82 ± 9 cells/mL), and *Skeletonema* spp. (68 ± 6 cells/mL) were the most abundant diatoms, *Heterocapsa* sp. (16 ± 4 cells/mL) was the most abundant dinoflagellate, cryptophytes were observed at concentrations of 175 ± 51 cells/mL, and euglenophytes were observed at concentrations of 5 ± 0 cells/mL.

DISCUSSION

This study assessed phytoplankton assemblage dynamics at the East River/LIS border following COVID-19 as they relate to fluctuations in N form and concentration. *In-situ* bioassays showed that DIN additions resulted in elevated cell concentrations of certain chain-forming diatom species as well as biomass increases in the smallest (<5 mm) phytoplankton size fraction, though the magnitude of these effects were often statistically nominal. These data were augmented by field sampling, which contextualized experimental observations within a phytoplankton community dominated

by picoplankton and diatoms. Analyses of publicly available nutrient data showed significant concentration decreases in some N forms during the COVID-19 stay-in-place orders.

Bioassay results indicated that ~20 μM increases in nitrate, ammonium, and urea had a disproportionate impact on the September 2021 Throgs Neck phytoplankton assemblage. For example, chl-*a* values at t(72) indicated the strongest impact of N form on the <5 μm size fraction (cyanobacteria). The significant decreases in the UP additions and ALL additions indicated that urea and phosphate did not limit cyanobacteria growth when compared to other N forms in this experiment. This is consistent with past research indicating that cyanobacteria rapidly uptake ammonia (Glibert et al. 2014). Urea is one of the simplest forms of organic N; historical fluctuations in Kjeldhal N suggest organic N at Throgs Neck can be both high and variable (Figure 2). The observed decreases in cyanobacterial biomass may be reflective of stochasticity due to high background levels of organic N.

The significant differences in final t(72) cell concentrations for *P. minimum* was likely an artifact of the low (1 cell/ mL) initial cell abundances. Significant differences in t(0) to t(24) growth rates of *Heterocapsa* sp. and *Gymnodinium* sp. may similarly be artifacts of low abundance (t(0) abundance 0 cells/mL and 3 cells/mL, data not shown). Cryptophytes displayed a strong growth increase in the UP addition (t(0) to t(24)) suggesting a preference for this N form; however, the t(24) to t(72) growth rate did not bear out this trend.

Phytoplankton counts at t(72) and analysis of growth rates indicate there may be similar trends between the growth of some diatoms as they relate to N-form at Throgs

Neck. Following analysis of differences in mean final cell concentrations across treatments, *Thalassiosira* spp. and *Guinardia* sp. (Table 4) both displayed similar relationships to N form. Though not statistically significant at $\alpha = 0.05$, NP, AP, and ALL additions exhibited higher cell concentrations than the control. Both taxa also displayed higher growth rates (t(24) to t(72)) in the presence of these N forms. Similar trends can be seen in the growth rate (t(24) to t(72)) of the diatom *Skeletonema* spp. Combined, these observations suggest that DIN accelerates growth rates of these and potentially other chain forming diatoms in this system; a study with a more replicates or fewer treatments (thus greater statistical power) may identify additional significant DIN-diatom associations. Comparatively, growth rates t(24) to t(72) of flagellated species (dinoflagellates, cryptophytes, and euglenophytes) were negative with few exceptions, suggesting that these organisms were outcompeted for nutrients in this experimental design. Contrary to published research, dinoflagellates were not found to have elevated growth in the presence of ammonia or urea (Heil et al. 2007), but this may simply be a result of low initial cell abundance or existing enrichment of these N forms.

Field counts in the study area (Table 2) indicate that the diatom populations at the East River/LIS border may have been decreasing through the months of July-September 2021, as *Thalassiosira* spp., *Skeletonema* spp., and *Guinardia* sp. consistently decreased in abundances during each sampling effort. A similar trend can be seen for dinoflagellate species, although cryptophytes displayed an increasing trend. Coupled with historical values of N form (Figure 2), this suggests that decreasing diatom concentrations correlate with increases in nitrate and nitrite approaching the fall. Further research should investigate the causality in this relationship: are diatom blooms driving nitrate and nitrite

levels or vice versa? Ammonium and Kjeldahl N do not display clear enough trends with their means to suggest similar speculative relationships with dinoflagellates and cryptophytes.

Although summer 2020 nitrate and nitrite values were not significantly different from historical means, the relatively low *p*-value (.086) during June 2020 suggested that concentrations may have been lower than typical during the period at the beginning of summer (Table 5) and potentially earlier that year. Ammonium values were significantly lower in both June and September 2020 than historical means ($p=.024$ and $p<.01$). These decreases (~5 μM) suggest that if COVID-19 stay-in-place orders did result in shifts in N form and concentration, it would be of a low magnitude at the East River/LIS confluence. The bioassay data presented herein only allows speculation on the additive impacts of N additions, but it appears that a 5 μM decrease in DIN may be too low to have a noticeable change in phytoplankton abundances and biomass (there were no striking patterns observed at 20 μM).

It's possible that linkages between N-form and phytoplankton growth were present but not detected, as power analysis ($n=3$ replicates across 6 treatments) indicated a high probability of Type-II error (~90%) at a medium effect size; however, greater replicates were neither financially nor logistically feasible. Nevertheless, results pave the way for future investigation. In particular, this study offers some support for a mechanistic linkage between DIN and diatom concentration at the WLIS and East River confluence. Since implementation of East River TMDL's in 2000, decreases in both DIN and diatom abundances have been observed at many WLIS water quality monitoring stations (Suter et al. 2014). Here, modest increases in the concentration of some diatoms

were seen with the addition of nitrate and ammonia while these DIN additions appeared to have no impact on dinoflagellate concentrations. This agrees with past research suggesting diatoms preferentially uptake nitrate from available N-forms (Song and Ward 2007; Oloffson et al. 2019). However, the observed increase in diatom concentration with the addition of ammonia contradicts studies in other systems where ammonia was shown to inhibit diatom growth (Glibert et al. 2014), suggesting these processes vary by location. Further research should aim to characterize ammonia uptake by *Thalassiosira* spp., *Skeletonema* spp., and *Guinardia* sp. in the WLIS, particularly in the competitive presence of cyanobacteria. Characterization of the biogeochemical conditions relating N form to diatom abundance may help refine management of TMDLs by elucidating which forms of N are most critical to continue to effectively reduce hypoxic area.

REFERENCES

Anderson, T.H., and G. Taylor. 2001. Nutrient pulses, plankton blooms, and seasonal hypoxia in Western Long Island Sound. Estuaries 24:228-243.

Anderson, D.M., J.M. Burkholder, W.P. Cochlan, P.M. Glibert, C.J. Gobler, C.A. Heil, and G.A. Vargo. 2008. Harmful algal blooms and eutrophication: examining linkages from selected coastal regions of the United States. Harmful Algae 8:39-53.

Armstrong, C.T., D.L., Erdner, J.W. McClelland, M.P. Sanderson, D.M. Anderson, C.J. Gobler, and J.L. Smith. 2018. Impact of nitrogen chemical form on the isotope signature and toxicity of a marine dinoflagellate. Marine Ecology Progress Series 602:63–76.

Bick, A., A. Blandin, and K. Mertens. 2020. Work from home before and after the Covid-19 outbreak. Federal Reserve Bank of Dallas Working Paper, 2017.

Connerton, P., J.V. Assuncao, R.M. de Miranda, A.D. Slovic, P.J. Pérez-Martínez, and H. Riberito. 2020. Air quality during COVID-19 in four megacities: lessons and challenges for Public Health. International Journal of Environmental Research and Public Health 15:5067.

Cira, E.K., H.W. Pearl, and M.S. Wetz. 2016. Effects of nitrogen availability and form on phytoplankton growth in a eutrophied estuary (Neuse River Estuary, NC, USA). PLoS One 11:e0160663.

Glibert, P.M., and C. Legrand. 2006. The diverse nutrient strategies of harmful algae: focus on osmotrophy. Pages 163-175 *in* Granéli, E., and Turner, J., editors. Ecology of harmful algae. Springer, Berlin.

Glibert, P.M., F.P. Wilkerson, R.C. Dugdale, A.E. Parker, J. Alexander, S. Blaser, and S. Murasko. 2014. Phytoplankton communities from San Francisco Bay Delta respond differently to oxidized and reduced nitrogen substrates—even under conditions that would otherwise suggest nitrogen sufficiency. Frontiers in Marine Science 1:17.

Gobler, C.J., A. Burson, F. Koch, Y. Tang, and M.R. Mulholland. 2012. The role of nitrogenous nutrients in the occurrence of harmful algal blooms caused by *Cochlodinium polykrikoides* in New York estuaries (USA). Harmful Algae 17:64-74.

Greenfield, D.I., D.J. Lonsdale, and R.M. Cerrato. 2005. Linking phytoplankton community composition with juvenile-phase growth in the Northern Quahog *Mercenaria*. Estuaries 28:241-251.

Griffith, A.W., S.E. Shumway, and C.J. Gobler. 2019. Differential mortality of North Atlantic bivalve molluscs during harmful algal blooms caused by the dinoflagellate,

Cochlodinium (aka Margalefidinium) *polykrikoides*. Estuaries and Coasts 42:190-203.

Grasshoff, K., K. Kremling, and M. Ehrhardt. 1999. Methods of seawater analysis. Wiley, Weinheim. 3rd edn.

Hales, B., A. van Geen, and T. Takahashi. 2004. High-frequency measurement of seawater chemistry: Flow-injection analysis of macronutrients. Limnology and Oceanography: Methods 2:91-101.

Hattenrath, T.K., D.M. Anderson, and C.J. Gobler. 2010. The influence of anthropogenic nitrogen loading and meteorological conditions on the dynamics and toxicity of *Alexandrium fundyense* blooms in a New York (USA) estuary. Harmful Algae 9:402-412.

Hattenrath-Lehmann, T.K., M.A. Marcoval, H. Mittlesdorf, J.A. Goleski, Z. Wang, B. Haynes, S.L. Morton, and C.J. Gobler. 2015. Nitrogenous nutrients promote the growth and toxicity of *Dinophysis acuminata* during estuarine bloom events. PLoS One 10:e0124148.

Hattenrath-Lehmann, T.K., R.J. Ossiboff, C.A. Burnell, C.D. Rauschenberg, K. Hynes, R.L. Burke, E.M. Bunting, K. Durham, and C.J. Gobler. 2017. The role of a PSP-producing Alexandrium bloom in an unprecedented diamondback terrapin (Malaclemys terrapin) mortality event in Flanders Bay, New York, USA. Toxicon 129:36-43.

Heil, C.A., M. Revilla, P.M. Glibert, and S. Murasko. 2007. Nutrient quality drives differential phytoplankton community composition on the southwest Florida shelf. Limnology and Oceanography 52:1067-1078.

Li, Y., S.L. Meseck, and M.S. Dixon. 2018. The East River tidal strait, New York City, New York, a high-nutrient, low-chlorophyll coastal system. International Aquatic Research 10:65-77.

Lopez, G., D. Carey, J.T. Carlton, R. Cerrato, H. Dam, R. Digiovanni, C. Elphick, F. Michael, C. Gobler, L. Hice, P. Howell, A. Jordaan, S. Lin, S. Liu, D. Lonsdale, M. Mcenroe, K. Mckown, G. Mcmanus, R. Orson, B. Peterson, C. Pickerell, R. Rozsa, S.E. Shumway, A. Siuda, K. Streich, S. Talmage, G. Taylor, E. Thomas, M. Van Patten, J. Vaudrey, C. Yarish, G.H. Wikfors, and R. Zajac. 2014. Biology and ecology of Long Island Sound. Pages 285-479 *in* Latimer, J.S., M.A. Tedesco, R.L. Swanson, C. Yarish, P.E. Stacey, and C Garza. Long Island Sound: Prospects for the Urban Sea. Springer, New York.

Long Island Sound Study. 2021. Long Island Sound- By the numbers. https://longislandsoundstudy.net/ (Accessed August 8, 2021).

Lonsdale, D.J., D.I. Greenfield, E.M. Hillebrand, R. Nuzzi and G.T. Taylor. 2006. Contrasting microplanktonic composition and food web structure in two coastal embayments (Long Island, NY, USA). Journal of Plankton Research 28:891-905.

New York City Department of Environmental Protection (NYC DEP). 2021. Harbor water quality. https://data.cityofnewyork.us/Environment/Harbor-Water-Quality/5uug-f49n (Accessed Aug 12, 2021)

O'Shea, M.L., and T.M. Brosnan. 2000. Trends in indicators of eutrophication in western Long Island Sound and the Hudson-Raritan estuary. Estuaries 23:877-901.

O'Donnell, J., R.E. Wilson, K. Lwiza, M. Whitney, W.F. Bohlen, D. Codiga, D.B. Fribance, T. Fake, M. Bowman, and J. Varekamp. 2014. The physical oceanography of Long Island Sound. Pages 79-158 *in* Latimer, J.S., M.A. Tedesco, R.L. Swanson, C. Yarish, P.E. Stacey, and C Garza. Long Island Sound: Prospects for the Urban Sea. Springer, New York.

Olofsson, M., E.K. Robertson, L. Edler, L. Arneborg, M.J. Whitehouse, and H. Ploug. 2019. Nitrate and ammonium fluxes to diatoms and dinoflagellates at a single cell level in mixed field communities in the sea. Scientific Reports 9:1-12.

Redfield, A.C. 1958. The biological control of chemical factors in the environment. American Scientist 46:205-221.

Reed, M., J. DiTullio, S. Kacenas, and D.I. Greenfield. 2015. Effects of nitrogen and dissolved organic carbon on microplankton abundances in four coastal South Carolina systems. Aquatic Microbial Ecology 76:1-14.

Reed, M.L., J.L. Pinckney, C.J. Keppler, L.M. Brock, S.B. Hogan, and D.I. Greenfield. 2016. The influence of nitrogen and phosphorus on phytoplankton growth and assemblage composition in four coastal, southeastern USA systems. Estuarine, Coastal, and Shelf Science 177:71-82.

Sitta, K., T. Callahan, C. Doll, R. Mortensen, M. Reed, and D.I. Greenfield. 2018. The influences of nitrogen form and zooplankton grazing on phytoplankton assemblages in two coastal southeastern systems. Limnology and Oceanography 63:2523-2544.

Siegel, A., B. Cotti-Rausch, D.I. Greenfield, and J. Pinckney. 2011. Nutrient controls of planktonic cyanobacteria abundance in coastal stormwater detention ponds. Marine Ecology Progress Series 434:15-27.

Song, B., and B.B. Ward. 2007. Molecular cloning and characterization of high-affinity nitrate transporters in marine phytoplankton. Journal of Phycology 43:542-552.

Suter, E.A., K.M. Lwiza, J.M. Rose, C. Gobler, and G.T. Taylor. 2014. Phytoplankton

assemblage changes during decadal decreases in nitrogen loadings to the urbanized Long Island Sound estuary, USA. Marine Ecology Progress Series 497:51-67.

Vaudrey, J. 2017. New York City's impact on Long Island Sound water quality technical report. Report to Save the Sound, New Haven, CT.

Vlahos, P., M.M. Whitney, C. Menniti, J.R. Mullaney, J. Morrison, and Y. Jia. 2020. Nitrogen budgets of the Long Island Sound estuary. Estuarine, Coastal, and Shelf Science 232:106493.

Whitney, M.M., and P. Vlahos. 2021. Reducing hypoxia in an urban estuary despite climate warming. Environmental Science and Technology 55:941-951.

Welschmeyer, N.A. 1994. Fluorometric analysis of chlorophyll a in the presence of chlorophyll b and phaeopigments. Limnology and Oceanography 39:1985-1992.

Yao, X., R.E. Sipler, B.C. Stanley, Q.N. Roberts, M.P. Sanderson, C.B. Bott, and D.A. Bronk. 2019. Quantifying effluent dissolved organic nitrogen (EDON) uptake by microbial communities along a salinity gradient in the York River. Estuaries and Coasts 42:1265-1280.

Zimmerman, C.F., and C.W. Keefe. 1991. Determination of nitrate + nitrite in estuarine and coastal waters by automated colorimetric analysis. An interim manual of methods for the determination of nutrients in estuarine and coastal waters. Revision, 1. EPA Method 353.4. Cincinnati, OH.